

MIT Open Access Articles

Digital CRISPR-based method for the rapid detection and absolute quantification of nucleic acids

The MIT Faculty has made this article openly available. **Please share** how this access benefits you. Your story matters.

Citation: Wu, Xiaolin, Tay, Joshua K, Goh, Chuan Keng, Chan, Cheryl, Lee, Yie Hou et al. 2021. "Digital CRISPR-based method for the rapid detection and absolute quantification of nucleic acids." *Biomaterials*, 274.

As Published: 10.1016/J.BIOMATERIALS.2021.120876

Publisher: Elsevier BV

Persistent URL: <https://hdl.handle.net/1721.1/143762>

Version: Original manuscript: author's manuscript prior to formal peer review

Terms of use: Creative Commons Attribution-NonCommercial-NoDerivs License



1 A Digital CRISPR-based Method for the Rapid Detection 2 and Absolute Quantification of Viral Nucleic Acids

3 Xiaolin Wu¹, Cheryl Chan¹, Yie Hou Lee¹, Stacy L. Springs^{1,2}, Timothy K.
4 Lu^{1,3,4,5,6,7,8*}, Harry Yu^{1,9,10,11*}

5 ¹Singapore-MIT Alliance for Research and Technology, Critical Analytics for
6 Manufacturing of Personalized Medicine Interdisciplinary Research Group,
7 Singapore 138602, Singapore

8 ²Center for Biomedical Innovation, Massachusetts Institute of Technology,
9 Cambridge, MA, USA.

10 ³Synthetic Biology Center, Massachusetts Institute of Technology (MIT),
11 Cambridge, MA 02139, USA

12 ⁴Synthetic Biology Group, Research Laboratory of Electronics, Massachusetts
13 Institute of Technology (MIT), Cambridge, MA 02139, USA

14 ⁵Broad Institute of MIT and Harvard, Cambridge, MA 02142, USA

15 ⁶Department of Electrical Engineering and Computer Science, Massachusetts
16 Institute of Technology (MIT), Cambridge, MA 02142, USA

17 ⁷Harvard-MIT Division of Health Sciences and Technology, Cambridge, MA
18 02139, USA

19 ⁸Department of Biological Engineering, Massachusetts Institute of Technology
20 (MIT), Cambridge, MA 02142, USA

21 ⁹Institute of Bioengineering and Nanotechnology, A*STAR, The Nanos, #04-
22 01, 31 Biopolis Way, Singapore 138669, Singapore

23 ¹⁰Mechanobiology Institute, National University of Singapore, T-Lab, #05-01,
24 5A Engineering Drive 1, Singapore 117411, Singapore

25 ¹¹Department of Physiology, The Institute for Digital Medicine (WisDM), Yong
26 Loo Lin School of Medicine, MD9-04-11, 2 Medical Drive, Singapore 117593,
27 Singapore

28 * Correspondence should be addressed to Timothy K. Lu (timlu@mit.edu) and
29 Harry Yu (phsyuh@nus.edu.sg).

30 **Abstract**

31 Quantitative real-time PCR and CRISPR-based methods detect SARS-CoV-2
32 in 1 hour but do not allow for the absolute quantification of virus particles,
33 which could reduce inter-lab variability and accelerate research. The 4-hour
34 reaction time of the existing digital PCR-based method for absolute virus
35 quantification is too long for widespread application. We report a Rapid Digital
36 Crispr Approach (RADICA) for the absolute quantification of SARS-CoV-2
37 DNA and Epstein–Barr virus DNA in human samples that yields results within
38 1 hour. For validation, we compared RADICA to digital PCR for quantifying
39 synthetic SARS-CoV-2 DNA and Epstein–Barr viral DNA. RADICA allows
40 absolute quantification of DNA with a dynamic range from 0.6 to 2027
41 copies/ μ L (R^2 value > 0.98), without cross-reactivity on similar virus or human
42 background DNA. Thus, RADICA can accurately detect and quantify nucleic
43 acid in 1h without thermal cycling, providing a 4-fold faster alternative to digital
44 PCR-based virus detection.

45 **Keywords:**

46 CRISPR, Molecular diagnosis, Absolute Quantification, SARS-CoV-2, virus
47 detection

48 **Introduction**

49 Methods to detect virus, as well as to quantify viral load, are needed for
50 diagnostics, therapeutics, and vaccines to combat the worldwide spread of
51 infectious disease, such as COVID-19. The reverse transcription-polymerase
52 chain reaction (RT-qPCR) is considered a gold standard for viral infection

53 diagnosis. However, quantification via RT-qPCR relies on the use of external
54 standards or references, and the results can be variable, with a 20–30%
55 variability reported even within trained laboratories¹⁻³. Thus, an absolute
56 quantification method with improved precision and accuracy is vital for virus
57 research⁴⁻⁶.

58 Digital PCR is increasingly being used as a highly accurate and sensitive
59 method for the absolute quantification of nucleic acids^{1, 7, 8}. In a digital PCR
60 reaction, the PCR mixture is separated into thousands of individual reactions,
61 resulting in the amplification of either zero or one of the nucleic acid target
62 molecules present in each partition. Since the PCR reaction in each partition
63 proceeds independently, absolute quantification by digital PCR is more
64 precise than RT-qPCR and more tolerant of inhibitors; furthermore, digital
65 PCR overcomes poor amplification efficiency¹. The sensitivity and precision of
66 digital PCR-based viral detection have been demonstrated in quantitative
67 detection and viral load analysis of SARS-CoV-2-infected patient samples
68 with reduced inter-lab variability and fewer false negatives and fewer false
69 positives compared with RT-PCR^{6, 9, 10}. In addition to its application in viral
70 diagnostics, digital PCR has also been applied to other areas of virus
71 research, including the study of the aerodynamic transmission of SARS-CoV-
72 2⁵. The main drawback of digital PCR, however, is the relatively long reaction
73 time (~4 hours) needed as a result of the 1-2°C/s ramp up/down rate for
74 efficient inter-partition heat transfer during thermal cycling, compared to that
75 of qPCR, which requires 1 hour. Reducing the reaction time of digital PCR is
76 therefore crucial in enabling the adoption of the technology for rapid virus
77 detection in hospitals and clinics¹¹.

78 Isothermal amplification methods, which amplify the nucleic acid target
79 molecule at a constant temperature and thereby reduce the reaction time,
80 have also been used for viral detection. These include methods that employ
81 recombinase polymerase amplification (RPA) or loop-mediated isothermal
82 amplification (LAMP)^{12, 13}. More recently, innovative diagnostic methods using
83 RNA-guided CRISPR/Cas system have been developed to detect nucleic
84 acids. In the RNA-guided CRISPR/Cas system, Cas effectors such as Cas12a
85 and Cas13a are exploited for their collateral cleavage activity, which refers to
86 the degradation of other nonspecific DNA/RNA oligos such as fluorescently-
87 tagged reporter oligos, once the Cas protein finds and cleaves a specific
88 DNA/RNA target^{14, 15}. By combining RPA- or LAMP-mediated isothermal
89 amplification of the target molecule with the CRISPR/Cas biosensing system,
90 methods such as SHERLOCK and DETECTR have detected dengue virus
91 and human papillomavirus, as well as SARS-CoV-2, in clinical samples¹⁶⁻²².
92 However, as CRISPR-based methods are not quantitative and require
93 multiple manipulations between the amplification and detection steps, there
94 remains a need for a quantitative, rapid, and robust viral detection method.

95 Here, we report the development of a digital CRISPR method for the rapid,
96 sensitive, and specific detection of viral nucleic acids at a constant
97 temperature. This method combines the advantages of quantitative digital
98 PCR, rapid isothermal amplification, and specific CRISPR detection into a
99 one-pot reaction system that partitions the individual reactions into 10,000
100 compartments on a commercial high-density chip. In this study, we
101 demonstrate an optimized Rapid Digital Crispr Approach (RADICA) that
102 allows for absolute quantification of viral nucleic acids at a constant

103 temperature in one hour. We validated this method using DNA containing the
104 N (nucleoprotein) gene of SARS-CoV-2 and showed a linear signal-to-input
105 response of R^2 value > 0.99 . We compared our RADICA detection system
106 against the traditional digital PCR method and show that the RADICA system
107 (1h vs 4h) was faster and had sensitivity and accuracy comparable to that of
108 traditional digital PCR. Also, this method is highly specific and do not have
109 cross activity on other similar virus or human background DNA. We also used
110 RADICA in the absolute quantification of Epstein–Barr virus from human B
111 cells (R^2 value > 0.98). Our rapid and sensitive RADICA allows for the
112 accurate detection and absolute quantification of viral nucleic acids in one
113 hour.

114 **Results**

115 **Design of RADICA**

116 Commercial chips for sample partitioning and matched fluorescence reader
117 for endpoint detection were used in RADICA²³. In this system, each CRISPR-
118 based reaction mix is sub-divided into 10,000 partitions on the chip, resulting
119 in an average partition volume of 1.336 nL. We first optimized the bulk
120 CRISPR reaction to achieve a one-copy-per-1.336 nL partition detection
121 sensitivity on the chip. This is equivalent to femtomolar detection sensitivity in
122 a bulk reaction. We selected the Cas12a homolog from *Lachnospiraceae*
123 *bacterium* ND2006 (LbCas12a) as it showed the highest signal-to-noise ratio
124 relative to other Cas12a homologs from a previous study¹⁷. To test if the
125 RADICA could detect viral DNA with femtomolar sensitivity without pre-
126 amplification, serially-diluted dsDNA (double stranded DNA) was incubated

127 with LbCas12a together with its CRISPR RNA (crRNA) and a reporter
128 (quenched fluorescent DNA). The sensitivity of detection using the CRISPR-
129 based method without pre-amplification in a bulk reaction was found to be 10
130 pM (Supplementary Fig. 1), which did not meet the femtomolar sensitivity
131 requirement of RADICA.

132 To increase the sensitivity of detection of the CRISPR-based method, an
133 isothermal amplification step was used. RPA was chosen for the isothermal
134 amplification step because its reaction temperature (25°C to 42°C) is
135 compatible with that of Cas12a (25°C to 48°C). This allowed for a one-step
136 digital RPA-CRISPR absolute quantification method that eliminates multiple
137 manipulations inherent in two-step CRISPR-based detection methods such as
138 SHERLOCK and DETECTR^{14, 15}. To avoid Cas12a-mediated cleavage of the
139 target molecule before amplification, we designed the crRNA to target single-
140 stranded DNA (ssDNA) that is generated only after amplification of the target
141 molecule (Fig. 1b)²². Another advantage of this method is the ease of
142 designing ssDNA-targeting crRNA over traditional dsDNA-targeting crRNA,
143 because the nuclease activity of Cas12a on ssDNA has been reported to be
144 independent of the presence of protospacer adjacent motif (PAM)²⁴.

145 The RADICA developed in this study is illustrated in Fig. 1a. Extracted DNA
146 samples are loaded onto on the chip by capillary action, and the reaction is
147 partitioned into 10,000 compartments, resulting in zero or one target molecule
148 in each compartment. To prevent spontaneous target amplification by RPA at
149 room temperature²⁵, the RPA-CRISPR reaction was prepared without the
150 addition of Mg²⁺, which is required for the polymerase activity. All reactions

151 were prepared on ice and samples were loaded within one minute to prevent
152 premature target amplification. The partitioned reactions were incubated in
153 isothermal water baths, heat blocks, or warm rooms. In each compartment
154 containing the target molecule (Fig. 1b), RPA initiates from one DNA strand
155 and subsequently exposes the crRNA-targeted ssDNA region on the other
156 strand. As the amplification proceeds, Cas12a cleaves the positive ssDNA
157 strand, triggering its collateral cleavage activity, which in turn cleaves the
158 proximal quenched fluorescent probe (ssDNA-FQ reporter) to generate a
159 fluorescence signal. At the same time, ongoing amplification of the other DNA
160 strand exponentially amplifies the target DNA, triggering more Cas12a
161 activation and increasing the fluorescence readout. The proportion of positive-
162 to-negative compartments is analyzed based on the endpoint fluorescence
163 measurement, and the copy number of the target nucleic acid is calculated
164 based on the Poisson distribution, allowing for absolute quantification of the
165 sample (Fig. 1a). Concurrent detection of compartments in each tube by the
166 Clarity™ Reader shortens detection time to within minutes.

167 **RADICA optimization**

168 To validate and optimize the RADICA, G-block DNA or plasmids containing
169 the SARS-CoV-2 N (nucleoprotein) gene region were used and primers and
170 crRNAs specific for the SARS-CoV-2 N gene were designed accordingly
171 based on previous studies²². The target regions overlap with those of the
172 China CDC assay (N gene region) with some modification to meet the primer
173 and crRNA design (Supplementary Table 1). To optimize the Cas12a-
174 mediated reaction, a bulk reaction using 0.1 nM and 1 nM dsDNA as a target

175 was performed with a range of Cas12a/crRNA concentrations. We found that
176 in the presence of a constant amount of target DNA and probe, comparable
177 fluorescence signal intensities were detected between 50 nM to 250 nM
178 Cas12a-crRNA concentrations, suggesting that changing the Cas12a/crRNA
179 concentration did not influence the reaction (Supplementary Fig. 2).

180 Since the quenched fluorescent probe is another key component that
181 influences the reaction, we optimized the FQ assay by incubating increasing
182 amounts of FQ probes with constant concentrations of Cas12a-crRNA and
183 target DNA. As expected, CRISPR-mediated fluorescence signal intensities
184 increased with increasing amounts of FQ probes (from 250 nM to 5 μ M),
185 although higher probe concentrations also resulted in higher background
186 noise (Fig. 2a,b). At FQ probe concentrations above 5 μ M, the signal-to-noise
187 ratio could not be further enhanced (Fig. 2b). To ensure that the fluorescence
188 signal generated on the partitioned chip was within the reader's detection
189 range, different FQ probe concentrations were tested in independent digital
190 CRISPR reactions in the presence of the target DNA and the fluorescence
191 measured on the digital PCR fluorescence reader. We found that in the
192 presence of the same target DNA, the proportions of positive partitions were
193 comparable regardless of the FQ probe concentration used (Fig. 2d).

194 However, only the background noise and positive signals generated in the
195 reaction with 500 nM FQ probe concentration were within the reader's
196 detection range, while the reactions containing 1000 nM FQ probe
197 concentration yielded higher background noises, which are difficult to
198 separate from positive signals (Fig. 2c). We therefore used 500 nM FQ probe

199 concentrations to achieve high signal-to-noise ratios for subsequent
200 experiments.

201 An additional optimization step involved developing a one-pot reaction that
202 combines the RPA and Cas12a reactions. We performed the bulk reaction at
203 25°C, 37°C and 42°C, which are temperatures within the reaction temperature
204 ranges of RPA (25°C to 42°C) and Cas12a (25°C to 48°C). First, we tested
205 the reaction using serial dilutions of plasmid DNA at 25°C and 42°C. The
206 reaction proceeded at both of these reaction temperatures, with a limit of
207 detection of about 9.4 copies/ μ L. However, at 25°C, the reaction proceeded
208 significantly more slowly with lower positive signals and a higher background
209 than the reaction performed at a 42°C (Supplementary Fig. 3). Next, we
210 assessed the effect of different temperatures (25°C, 37°C and 42°C) on
211 reactions containing a constant amount of plasmid DNA (37.5 copies/ μ L). We
212 found that higher temperatures accelerated the reaction (Supplementary Fig.
213 3c). Taken together, our results suggest that 42°C is the optimal temperature
214 for the RPA-Cas12a reaction.

215 We next investigated whether the reaction time affected the precision of
216 RADICA on plasmid DNA detection at 42°C. As shown in Fig. 3a, the reaction
217 proceeded quickly with some fluorescence signal detected in several
218 compartments at 20 min, but with a low signal-to-noise ratio at this time point.
219 As the reaction proceeded, two distinct peaks indicating the negative (left) and
220 positive (right) partitions were detected at 40 min (Fig. 3a). Analysis of the
221 ratio of positive partitions on the chip at the different time points revealed that
222 the number of positive partitions reached a plateau after 60 min in all four

223 replicates, suggesting that 60 min was the earliest end-point measurement
224 (Fig. 3b). All subsequent experiments were therefore performed for 60
225 minutes.

226 **Absolute quantification of SARS-CoV-2 DNA using RADICA**

227 We next characterized the assay performance of RADICA in detecting and
228 quantifying SARS-CoV-2 and compared it to that of digital PCR. In this assay,
229 linearized plasmid containing the SARS-CoV-2 N gene was serially diluted
230 and used as the target DNA in the aforementioned optimized RADICA or
231 digital PCR reactions. Using RADICA-based detection, a proportional
232 increase in the number of positive partitions was observed with increasing
233 concentrations of the target DNA (Fig. 4a), indicating the good quantitative
234 performance of RADICA. Although few partitions in the negative control were
235 classified as having a positive signal due to non-specific amplification, the
236 average of 10 negative control replicates give us an average of 0.165
237 copies/ μ L readout and the limit of blank (LoB) is 0.413 copies/ μ L, which is
238 about half of our limit of detection (LoD), 0.897 copies/ μ L (Fig. 4a,
239 Supplementary Table 2).

240 To test the robustness and reproducibility of RADICA, at least ten
241 independent RADICA reactions using the SARS-CoV-2 N gene as the target
242 DNA were performed on different days. The coefficient of variation (CV)
243 observed for most samples was $\leq 15\%$ except for the lowest dilution (0.6
244 copies/ μ L), indicating the limit of quantification (LoQ) of this method is around
245 2.2 copies/ μ L of the viral genome (Supplementary Table 2). To assess the
246 accuracy of RADICA-based nucleic acid detection against that of digital PCR,

247 DNA concentrations measured by RADICA were plotted against the
248 corresponding DNA concentrations obtained by digital PCR. Linear regression
249 analysis revealed an R^2 value of above 0.99 across a dynamic range from 0.6
250 to 2027 copies/ μ L, suggesting that RADICA was reliable for the absolute
251 quantification of nucleic acids (Fig. 4b). These data highlight the sensitivity,
252 accuracy, and speed of the digital CRISPR-based detection method
253 developed in this study for the absolute quantification of nucleic acids in
254 samples.

255 **Accuracy analysis of RADICA-based quantification on circular plasmid**

256 Plasmids are routinely used as reference DNA or standards in many analytical
257 DNA measurements. However, conformational changes in supercoiled DNA
258 have been reported to have a profound effect on PCR-based quantification²⁶⁻
259 ²⁸. Unsuccessful single-molecule amplification of non-linearized plasmids was
260 reported in a PCR-based study, which resulted in an underestimation for
261 circular plasmid quantification on some dPCR machines^{29, 30}. To test whether
262 plasmid conformation also affects the accuracy of RADICA, undigested
263 plasmid containing the SARS-CoV-2 N gene was serially diluted and used for
264 digital PCR or RADICA reactions. Concentrations of non-linearized plasmids
265 measured by digital PCR were about half of those detected for linearized
266 plasmids (regression coefficients at 0.5261) (Fig. 5d), which is in accordance
267 with previous studies and indicates that the accuracy of digital PCR is
268 influenced by plasmid conformation. Compared to digital PCR, RADICA
269 showed higher amplification efficiency of the supercoiled plasmid DNA, as
270 evidenced by the higher positive compartments ratio detected (Fig. 5a,b).

271 RADICA concentrations of non-linearized plasmids were highly concordant
272 with those of linearized plasmids (regression coefficients at 1.0673) (Fig. 5c),
273 suggesting that the accuracy of RADICA is not affected by plasmid
274 conformation.

275 **Specificity analysis of RADICA-based detection**

276 Primer and crRNA designs are key in determining the specificity of CRISPR-
277 based nucleic acid detection assays. Previous studies have shown the ability
278 of RPA to tolerate up to nine nucleotide base-pair mismatches across primer
279 and probe binding sites²⁵. To specifically detect SARS-CoV-2 using RADICA,
280 primers and crRNAs must be designed to specifically bind the SARS-CoV-2
281 target DNA and not its closely-related coronaviruses, such as MERS-CoV and
282 other related human coronaviruses. We first analysed the binding sites of the
283 primers and crRNAs that were originally designed based on the consensus
284 sequence of the genome of 264 SARS-CoV-2 strains, available on the
285 GISAID database^{22, 31, 32}. The consensus sequence of these SARS-CoV-2
286 target regions was aligned with corresponding regions of SARS-CoV-2-related
287 beta coronaviruses, such as SARS-CoV, MERS-CoV, and human
288 coronaviruses Human-CoV 229E/HKU1/NL63/OC43. No cross-binding
289 regions were observed with the other SARS-CoV-2-related coronavirus
290 analyzed (Supplementary Fig. 4a). A comparison between the binding site
291 sequences of SARS-CoV-2 and its most similar relative, SARS-CoV, showed
292 that there were 13 sequence variations across the primer and crRNA binding
293 sites (three, two, and seven sequence variations at the forward primer,
294 reverse primer, and crRNA binding site, respectively). This is more than the

295 nine nucleotide base-pair mismatch tolerance threshold for RPA, which
296 therefore predicts the specificity of the designed primers and crRNA for
297 SARS-CoV-2-specific CRISPR-based detection. To test the specificity of the
298 reaction, we assayed the bulk RPA-Cas12a reaction using target plasmids
299 containing the complete N gene from SARS-CoV-2, SARS-CoV, and MERS-
300 CoV (Supplementary Fig. 4b,c). Positive fluorescence signals were observed
301 only in the reaction containing the SARS-CoV-2 plasmid, not in reactions
302 containing SARS-CoV and MERS-CoV plasmids (Supplementary Fig. 4b,c).
303 The absence of cross-reactivity with the other related coronaviruses tested in
304 this study validates the specificity of the CRISPR assay for SARS-CoV-2.

305 **Background human DNA tolerance analysis of RADICA**

306 Previous studies have reported that RPA reactions could be inhibited by high
307 concentrations of background human DNA^{33, 34}. We therefore first tested the
308 RPA-Cas12a bulk reaction in the presence of various concentrations of
309 background human DNA (Supplementary Fig. 5). In an RPA-Cas12a reaction
310 with 37.5 copies/ μ L of target DNA, background human DNA concentrations
311 below 2 ng/ μ L did not affect the reaction (Supplementary Fig. 5a).

312 Concentrations of background human DNA above 5 ng/ μ L in a bulk RPA-
313 Cas12a reaction showed reduced fluorescent signal intensities, which is in
314 agreement with the inhibitory concentrations of background DNA reported in
315 previous studies using bulk RPA reactions³⁴ (Supplementary Fig. 5a).

316 We also tested for possible inhibitory effects of background DNA on reactions
317 carried out in small partitions. In an RPA-Cas12a reaction with 400 copies/ μ L
318 of target DNA, 1 ng/ μ L of background human DNA (equivalent to about 4350

319 human cells per reaction) did not affect the RADICA reaction (Supplementary
320 Fig. 5b). We also observed inhibition of the reaction containing 2 ng/ μ L of
321 background human DNA, and complete inhibition of the reaction containing >5
322 ng/ μ L of background human DNA (Supplementary Fig. 5b). Nevertheless,
323 since input DNA concentrations used for RADICA-based detection are
324 typically below 1 ng/ μ L, our findings suggest that background DNA will not
325 inhibit the RADICA reaction of samples within the dynamic range to be used
326 for testing.

327 Previous studies have also reported that the tolerance of RPA for background
328 DNA is dependent on target DNA concentrations present in the reaction^{33, 34}.
329 We therefore tested the effect of 1 ng/ μ L of background human DNA
330 (equivalent to about 4350 human cells per reaction) on RADICA reactions
331 with various concentrations of target DNA (Supplementary Fig. 5c). Our
332 results show that 1 ng/ μ L of background DNA did not affect reactions that
333 contained target DNA concentrations within the dynamic range of digital PCR
334 detection, i.e., 0.6 to 2027 copies/ μ L (Supplementary Fig. 5c). Our findings
335 confirm that the presence of background human DNA in the sample is not
336 likely to affect the absolute quantification of RADICA.

337 **RADICA detection and absolute quantification of SARS-CoV-2 RNA**

338 As SARS-CoV-2 is an RNA virus, we next tested whether RADICA could be
339 combined with reverse transcription (RT) in a one-pot reaction for the absolute
340 quantification of RNA. RNA corresponding to the SARS-CoV-2 gene N target
341 region was synthesized using a T7 promoter-tagged PCR product and T7
342 RNA polymerase, and different concentrations of RNA were tested in bulk RT-

343 RPA-Cas12a reactions. Our results show a lower-than-expected sensitivity of
344 the one-pot RT-RPA-Cas12a bulk reaction, with a detection limit at 244
345 copies/ μ L (Supplementary Fig. 6b). To assess if this decrease in sensitivity
346 was in part due to an inefficient reverse transcription process in the one-pot
347 reaction, we employed two reverse primers to facilitate the reverse
348 transcription reaction and increase the sensitivity of the one-pot reaction. We
349 detected an increase in sensitivity of 61 copies/ μ L when two reverse primers
350 were used (Supplementary Fig. 6c).

351 We tested the sensitivity of the one-pot RT-RPA-Cas12a reaction in small
352 partitions on RADICA using varying concentrations of RNA. Notably, although
353 the positive partition proportion increased with an increase in the
354 concentration of input RNA, 1 copy of input RNA resulted in an increase of
355 only 0.0177 copy as calculated by RADICA, suggesting that the RADICA does
356 not accurately quantify RNA (Supplementary Fig. 6d). Although the addition of
357 two reverse primers increased the signal, it was insufficient to achieve a one-
358 copy-per-partition sensitivity (Supplementary Fig. 6e). Our findings suggest
359 that absolute quantification of RNA by RADICA may require prior conversion
360 to cDNA before the sample is analysed on a digital chip.

361 **Absolute quantification of Epstein–Barr virus via RADICA**

362 Having demonstrated the accuracy of RADICA on SARS-CoV-2 DNA
363 samples, we tested the ability of our RADICA method to perform absolute
364 quantification of Epstein–Barr virus (EBV) DNA samples. To design primers
365 and crRNA that were universal to both type I and type II EBV, the genomes
366 of 16 EBV strains were analysed to identify conserved regions across all 16

367 EBV strains. A conserved DNA region within the Epstein-Barr nuclear antigen
368 1 (EBNA1) was used as the target sequence (Fig. 6a). Viral DNA extracted
369 from chemically-induced EBV-harboring human B cells was diluted to
370 concentrations ranging from 0.5 to 2100 copies/ μ L, and used as the target
371 DNA in both RADICA and digital PCR reactions. In the RADICA-based
372 detection, samples loaded in the partition chip were incubated for 1 h at
373 42 °C, followed by endpoint fluorescence detection and copy number
374 determination. Notably, the positive partition signal increased with an increase
375 in the concentration of input EBV DNA (Fig. 6b). The copy numbers measured
376 by RADICA were in full agreement (R^2 value > 0.98) with those measured by
377 digital PCR (Fig. 6c). Our findings validate the accuracy and sensitivity of our
378 RADICA for the absolute quantification of viral DNA rapidly within an hour,
379 which is a 4-fold reduction in reaction time compared to digital PCR-based
380 detection.

381 **Discussion**

382 In our study, we have developed a rapid and accurate digital CRISPR method
383 for the absolute quantification of viral DNA. The performance characteristics
384 of this method were validated using SARS-CoV-2 synthetic DNA and EBV
385 DNA, and compared to those of absolute quantification digital PCR method,
386 the current gold standard. Our RADICA achieved sensitivity and detection
387 limits (LoD 0.897 copy/ μ L) comparable with those of qPCR and other
388 isothermal methods, such as SHERLOCK and DETECTR, with the ability of
389 absolute quantification (Supplementary Table 3). The significant advantage of
390 RADICA over dPCR is its speed: RADICA can perform absolute quantification

391 rapidly within an hour, which is four times faster than current dPCR-based
392 detection.

393 Absolute quantification for viral detection could not only facilitate clinical
394 processing but also benefit research. Viral loads closely parallel transmission
395 risk and disease severity. High SARS-CoV-2 viral loads have been reported to
396 correlate with the course of infection and mortality^{6, 35-38}. These reports
397 underscore the urgent need for rapid and sensitive virus detection and
398 quantification methods to monitor viral load as the basis for clinical decision
399 making. Such methods are also needed for mechanistic studies, transmission
400 studies, vaccine development, and therapeutics for COVID-19. Although there
401 currently exist many diagnostic methods available for virus detection, these
402 methods usually do not allow for a rapid and precise quantification of the viral
403 load (Supplementary Table 3).

404 RADICA reported in the study is four times faster than the traditional digital
405 PCR-based methods used for the absolute quantification of nucleic acids.
406 Additionally, the isothermal feature of RADICA-based detection assay confers
407 faster amplification of the viral target using a simple constant-temperature
408 heat bath, enabling rapid viral detection that can be deployed even in low-
409 resource areas. In recent years, other digital isothermal methods, such as
410 RPA- or LAMP-based digital PCR methods, have been developed for
411 detecting a variety of DNA targets³⁹⁻⁴¹. However, these methods are limited
412 by their low specificity, due to the inherent tolerance of RPA/LAMP-based
413 methods for base-pair mismatches as compared to traditional PCR methods⁴²⁻
414 ⁴⁴. Our RADICA overcomes this by exploiting the specificity conferred by the

415 Cas12a-crRNA-based targeting system. The collateral cleavage activity of
416 Cas12a amplifies the signal and thus increases the sensitivity.

417 Another advantage of RADICA over other CRISPR-based methods¹⁶⁻²¹ is its
418 one-pot reaction design, which reduces manual manipulation and increases
419 reproducibility. In this streamlined one-pot reaction, both nucleic acid
420 amplification and CRISPR-based detection are combined into a single step in
421 a closed tube, significantly reducing the risk of cross-contamination between
422 samples during batch processing. A major drawback of current CRISPR-
423 based methods is the complexity of designing appropriate crRNAs that are
424 limited to target regions in proximity to a PAM. This limitation may potentially
425 complicate CRISPR-based virus detection since mutations in the viral PAM
426 sequence may disable recognition by the Cas protein as the virus evolves. In
427 contrast, our simpler digital CRISPR crRNA design is independent of the PAM
428 sequence because it targets single-stranded DNA generated after
429 amplification²⁴.

430 RADICA reported here uses commercially available chips and devices that
431 can potentially be adapted to other devices already in use at some hospitals
432 and service laboratories. These are QuantStudio 3D Digital PCR System
433 (Thermo Fisher), QIAcuity Digital PCR System (QIAGEN), and Droplet Digital
434 PCR System (Bio-Rad). We therefore envisage greater ease of adoption of
435 our technology at these facilities. Furthermore, RADICA offers a potentially
436 customizable solution that is amenable to other DNA isothermal amplification
437 platforms such as loop-mediated isothermal amplification, rolling circle
438 amplification, and strand displacement amplification technologies, as well as

439 the use of other Cas proteins, such as Cas13a, Cas12b, Cas14 for multiplex
440 detection.

441 We have established and characterized RADICA, which combines the speed
442 and sensitivity of isothermal amplification, the specificity of CRISPR-based
443 detection, and the ability to obtain absolute quantification by sample
444 partitioning. Our RADICA detects a concentration of viral DNA as low as
445 0.897 copy/ μ L and enables rapid, absolute quantification with a dynamic
446 range of 0.6 to 2027 copies/ μ L within one hour at a constant temperature, with
447 no cross-reactivity to other similar viruses. Future work will focus on
448 expanding the applications of RADICA to areas such as gene expression
449 analysis, rare mutant detection, copy number variation, and sequencing
450 library quantification. Applications of such rapid analytics will also benefit cell
451 therapy, pharmaceutical, environmental, public health, security and food
452 industry to potentially determine the replication competency of adventitious
453 agents.

454 **Materials and methods**

455 **Materials**

456 Preparation of primers and DNA targets: Oligonucleotides (primers), ssDNA-
457 FQ reporters, SARS-CoV-2 N gene-containing G-Block, SARS-CoV-2, SARS-
458 CoV, and MERS N gene-containing plasmids were synthesized by or
459 purchased from Integrated DNA Technologies. The SARS-CoV-2 N gene-
460 containing plasmid was linearized using FastDigest Scal (Thermo Scientific)
461 and then used as DNA target. The SARS-CoV-2 N gene-containing plasmid
462 was used as a template to amplify the N gene using primer N-RNA-F/ N-RNA-

463 R by Platinum™ SuperFi II PCR Master Mix (Invitrogen). The PCR product
464 was purified by QIAquick PCR Purification Kit (QIAGEN) and used as RNA
465 synthesis template.

466 Synthetic RNA target preparation: Since N-RNA-F has a T7 promoter
467 sequence, the amplified DNA using N-RNA-F/R primer will contain a T7
468 promoter upstream of gene N. The T7 tagged N gene dsDNA was transcribed
469 into SARS-CoV-2 RNA using HiScribe™ T7 High Yield RNA Synthesis Kit
470 (New England Biolabs) according to the manufacturer's protocol. The
471 synthesized RNA was purified using Monarch® RNA Cleanup Kit (New
472 England Biolabs) after treatment with DNase I (RNase-free, New England
473 Biolabs).

474 crRNA preparation: Constructs were ordered as DNA from Integrated ssDNA
475 Technologies with an appended T7 promoter sequence. crRNA ssDNA was
476 annealed to a short T7 primer (T7-3G IVT primer⁴⁵ or T7-Cas12scaffold-F⁴⁶)
477 and treated with fill-in PCR (Platinum™ SuperFi II PCR Master Mix) to
478 generate the DNA templates. These DNA were used as templates to
479 synthesize crRNA using the HiScribe™ T7 High Yield RNA Synthesis Kit
480 (New England Biolabs) according to published protocols^{45, 46}. The synthesized
481 crRNA was purified using Monarch® RNA Cleanup Kit (New England Biolabs)
482 after treatment with DNase I (RNase-free, New England Biolabs),
483 Thermolabile Exonuclease I (New England Biolabs), and T5 Exonuclease
484 (New England Biolabs).

485 **Primer and crRNA design**

486 SARS-CoV-2 primers and crRNA were designed based on previously
487 published papers²² or 264 SARS-CoV-2 genome sequences from GISAID³¹.
488 ³². Other human-related coronavirus sequences were downloaded from NCBI.
489 UGENE software was used to analyze and align viral genomes (MUSCLE or
490 Kalign). Consensus sequences (Threshold: 90%) of 264 SARS-CoV-2
491 genomes, 328 SARS-CoV, 572 MERS-CoV, 70 Human-CoV-229E genomes,
492 48 Human-CoV-HKU1 genomes, 71 Human-CoV-NL63, and 178 Human-
493 CoV-OC43 were exported separately from UGENE and used for specificity
494 analysis.

495 Epstein–Barr virus primers and crRNA were designed based on consensus
496 sequences of 16 virus genomes including both type I and type II EBV
497 (NCBI: AP015016.1, AY961628.3, HQ020558.1, JQ009376.2, KC207813.1,
498 KC207814.1, KC440851.1, KC440852.1, KC617875.1, KF373730.1,
499 KF717093.1, KP735248.1, LN827800.1, NC_007605.1, NC_009334.1,
500 V01555.2).

501 **Digital PCR quantification**

502 SARS-CoV-2 N gene quantification: The G-block, plasmid, dsDNA and RNA
503 concentrations were quantified by digital PCR. Serial dilutions of targets were
504 mixed together with 500 nM CHNCDC-geneN-F, 500 nM CHNCDC-geneN-R,
505 250 nM CHNCDC-geneN-P, 1x TaqMan™ Fast Virus 1-Step Master Mix (for
506 RNA, Applied Biosystems) or TaqMan™ Fast Advanced Master Mix (for DNA,
507 Applied Biosystems), 1x Clarity™ JN solution (JN Medsys). For RNA
508 samples, the reaction mixture was incubated at 55°C 10 min before
509 partitioning the reaction mix on Clarity™ autoloader. Then the reaction

510 partitions were sealed with the Clarity™ Sealing Enhancer and 230 µL
511 Clarity™ Sealing Fluid, followed by thermal cycling using the following
512 parameters: 95 °C for 15 min (one cycle), 95 °C 50 s and 56 °C 90 s (40
513 cycles, ramp rate = 1 °C/s), 70 °C 5 min. The endpoint fluorescence of the
514 partitions was detected using Clarity™ Reader and the final DNA copy
515 numbers were analyzed by Clarity™ software.

516 EBV quantification: Serial dilutions of EBV DNA was used for dPCR
517 quantification by Clarity™ Epstein-Barr Virus Quantification Kit (JN Medsys)
518 according to the manufacturer's protocol.

519 **Cas12a bulk assay without preamplification**

520 Unless otherwise indicated, 50 nM EnGen® Lba Cas12a (New England
521 Biolabs), 50 nM crRNA, and 250 nM FQ ssDNA probe were incubated with
522 dsDNA dilution series in NEB buffer 2.1 at 37°C, and fluorescence signals
523 were measured every 5 min.

524 **RPA-Cas12a bulk assay**

525 The one-pot reaction combining RPA-DNA amplification and Cas12a
526 detection was performed as follows: 300 nM forward primer, 300 nM reverse
527 primer, 500 nM FQ probe, 1x RPA rehydration buffer containing 1 x RPA
528 Pellet (TwistDx), 200 nM EnGen® Lba Cas12a (New England Biolabs), 200
529 nM crRNA, were prepared followed by adding various amounts of DNA input,
530 and 14 mM magnesium acetate. When RNA was used as a target, 300 nM
531 reverse primer 2 was used with 10 U/µL PhotoScript Reverse transcriptase
532 (New England Biolabs) or 10 U/µL SuperScript™ IV Reverse Transcriptase

533 (Invitrogen) and 0.5 U/ μ L RNase H (Invitrogen or New England Biolabs), as
534 indicated. The reaction mixture was incubated at 42°C unless otherwise
535 indicated and fluorescence kinetics were monitored every 1 min.

536 **RADICA quantification**

537 The RADICA reaction was prepared by adding 1x Clarity™ JN solution (JN
538 Medsys) to the RPA-Cas12a bulk reactions stated above. 15 μ L of the mixture
539 was loaded on the chip by a Clarity™ autoloader for sample partitioning. The
540 reaction partitions were sealed with the Clarity™ Sealing Enhancer and 230
541 μ L Clarity™ Sealing Fluid, followed by incubation at 42°C for 1 hour, unless
542 otherwise indicated. After incubation, a Clarity™ Reader was used to read the
543 fluorescent signal in the partitions, and Clarity™ software was used to
544 calculate input DNA copy numbers.

545 **Limit of Blank (LoB), Limit of Detection (LoD), and Limit of Quantitation** 546 **(LoQ) calculation**

547 LoB, LoD, and LoQ were calculated based on the following equation⁴⁷ using
548 the statistics of RADICA quantification on linearized plasmid in 10 replications
549 (Supplementary Table 2):

$$550 \text{ LoB} = \text{mean}_{\text{blank}} + 1.645 (\text{SD}_{\text{blank}})$$

$$551 \text{ LoD} = \text{LoB} + 1.645 (\text{SD}_{\text{low concentration sample}})$$

$$552 \text{ LoQ} = \text{the lowest concentration of CV} \leq 20\%$$

553 **Growing EBV-2 from Jijoye cells**

554 Jijoye cells were treated with 4 mM sodium butyrate and 24 ng/ml
555 tetradecanoyl phorbol acetate (TPA). Supernatants were harvested 4-5 days
556 post-treatment by centrifugation at 4,000g for 20 min and passing over a 0.45
557 µm filter to remove cellular debris. Viral particles were pelleted by
558 ultracentrifugation at 20,000 rpm for 90 min and resuspended in 1/100 the
559 initial volume using complete RPMI or PBS if viruses were to be further
560 purified. Concentrated viruses were further purified using OptiPrep gradient
561 density ultracentrifugation at 20,000 rpm for 120 min, and the virus interface
562 band collected and stored at -80°C for downstream analysis.

563 **Epstein–Barr virus DNA extraction**

564 EBV DNA was extracted using QIAamp DNA Mini Kit (QIAGEN) according to
565 the manufacturer's protocol.

566 **Acknowledgments**

567 We thank Karen Pepper (MIT) and Scott A. Rice(NTU) for careful editing and
568 helpful comments on the manuscript. This research is supported by the
569 National Research Foundation, Prime Minister's Office, Singapore under its
570 Campus for Research Excellence and Technological Enterprise (CREATE)
571 programme, through Singapore MIT Alliance for Research and Technology
572 (SMART): Critical Analytics for Manufacturing Personalised-Medicine (CAMP)
573 Inter-Disciplinary Research Group.

574 **Author Contributions**

575 X.W., T.K.L., and H.Y. designed the research. X.W. developed the RADICA,
576 performed the experiment, and analyzed the data. C.C performed the

577 Epstein–Barr virus culture and DNA extraction. Y.H.L., S.S., T.K.L., and H.Y.
578 provided mentorship and feedback. X.W. wrote the original draft and all
579 authors reviewed and edited the manuscript.

580 **Competing Interests statement**

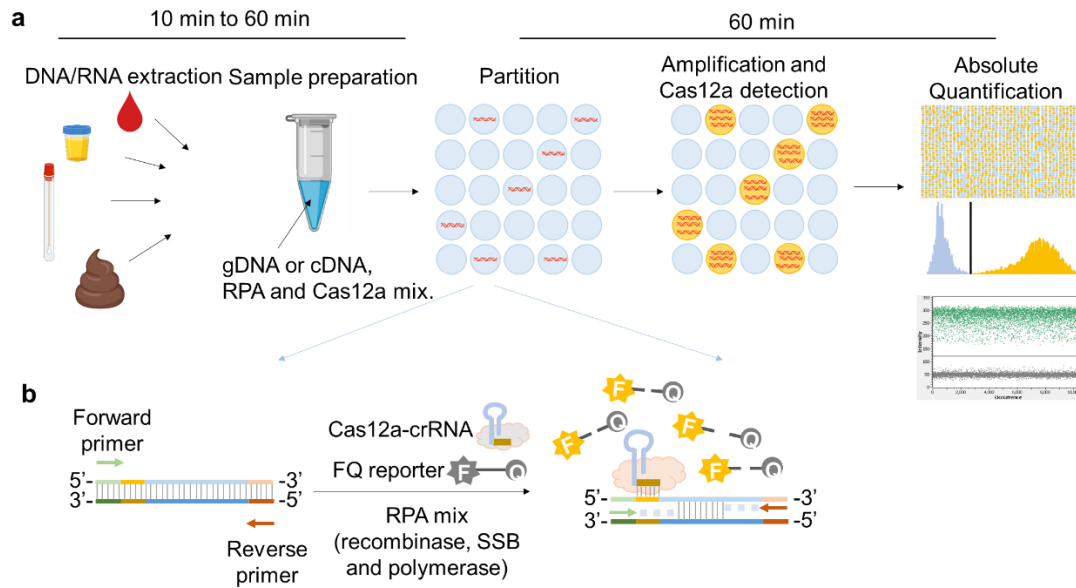
581 X.W., T.K.L., and H.Y. are co-inventors on patent filings related to the
582 published work. T.K.L. is a co-founder of Senti Biosciences, Synlogic, Engine
583 Biosciences, Tango Therapeutics, Corvium, BiomX, Eligo Biosciences,
584 Bota.Bio, and Avendesora. T.K.L. also holds financial interests in nest.bio,
585 Amplphi, IndieBio, MedicusTek, Quark Biosciences, Personal602Genomics,
586 Thryve, Lexent Bio, MitoLab, Vulcan, Serotiny, and Avendesora. H.Y.
587 declares holding equity in Invitrocue, Osteopore, Histoindex, Vasinfuse, Ants
588 Innovate, Synally Futuristech and Pishon Biomedical that have no conflict of
589 interest with the work reported in this paper.

590 **References**

- 591 1. Sedlak, R.H. & Jerome, K.R. Viral diagnostics in the era of digital polymerase
592 chain reaction. *Diagnostic microbiology and infectious disease* **75**, 1-4 (2013).
- 593 2. Lai, K.K., Cook, L., Wendt, S., Corey, L. & Jerome, K.R. Evaluation of real-
594 time PCR versus PCR with liquid-phase hybridization for detection of
595 enterovirus RNA in cerebrospinal fluid. *Journal of clinical microbiology* **41**,
596 3133-3141 (2003).
- 597 3. Boeckh, M. et al. Optimization of quantitative detection of cytomegalovirus
598 DNA in plasma by real-time PCR. *Journal of clinical microbiology* **42**, 1142-
599 1148 (2004).
- 600 4. Yao, X.-H. et al. Pathological evidence for residual SARS-CoV-2 in pulmonary
601 tissues of a ready-for-discharge patient. *Cell research* **30**, 541-543 (2020).
- 602 5. Liu, Y. et al. Aerodynamic analysis of SARS-CoV-2 in two Wuhan hospitals.
603 *Nature* **582**, 557-560 (2020).
- 604 6. Yu, F. et al. Quantitative Detection and Viral Load Analysis of SARS-CoV-2 in
605 Infected Patients. *Clinical Infectious Diseases* (2020).
- 606 7. Salipante, S.J. & Jerome, K.R. Digital PCR—An Emerging Technology with
607 Broad Applications in Microbiology. *Clinical chemistry* **66**, 117-123 (2020).
- 608 8. Whale, A.S. et al. Comparison of microfluidic digital PCR and conventional
609 quantitative PCR for measuring copy number variation. *Nucleic acids*
610 *research* **40**, e82-e82 (2012).

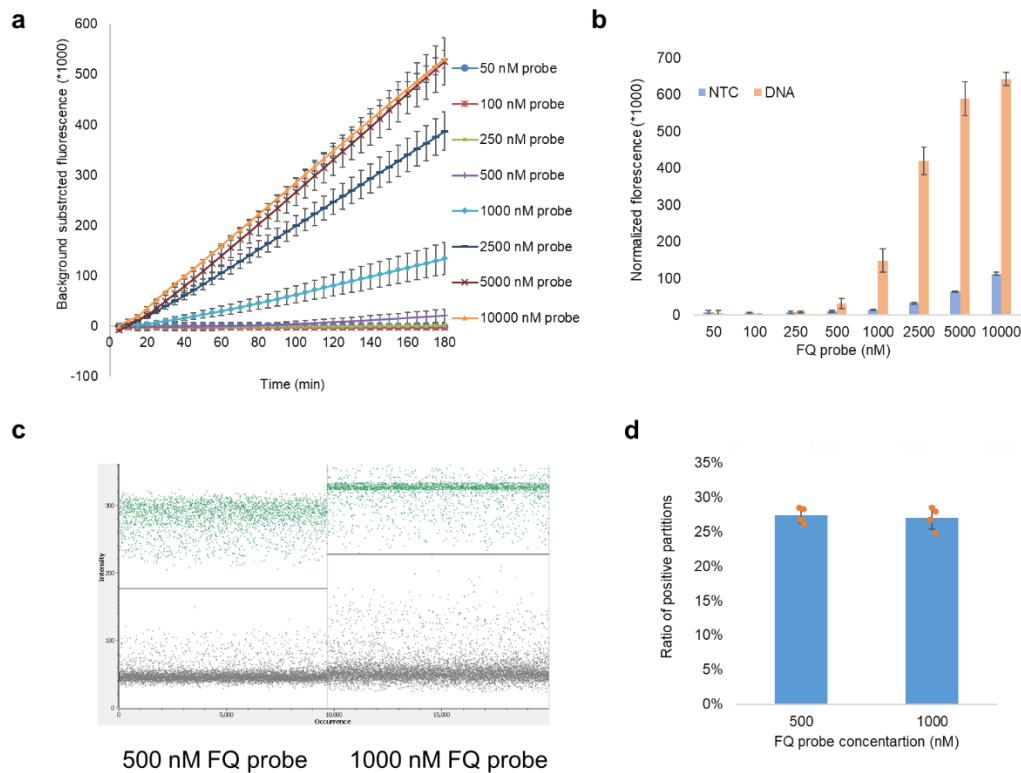
- 611 9. Liu, X. et al. Analytical comparisons of SARS-COV-2 detection by qRT-PCR
612 and ddPCR with multiple primer/probe sets. *Emerging microbes & infections*
613 **9**, 1175-1179 (2020).
- 614 10. Alteri, C. et al. Detection and quantification of SARS-CoV-2 by droplet digital
615 PCR in real-time PCR negative nasopharyngeal swabs from suspected
616 COVID-19 patients. *PLoS one* **15**, e0236311 (2020).
- 617 11. Woloshin, S., Patel, N. & Kesselheim, A.S. False Negative Tests for SARS-
618 CoV-2 Infection — Challenges and Implications. *New England Journal of*
619 *Medicine* **383**, e38 (2020).
- 620 12. Notomi, T. et al. Loop-mediated isothermal amplification of DNA. *Nucleic*
621 *acids research* **28**, E63-E63 (2000).
- 622 13. Piepenburg, O., Williams, C.H., Stemple, D.L. & Armes, N.A. DNA Detection
623 Using Recombination Proteins. *PLOS Biology* **4**, e204 (2006).
- 624 14. Gootenberg, J.S. et al. Nucleic acid detection with CRISPR-Cas13a/C2c2.
625 *Science* **356**, 438-442 (2017).
- 626 15. Chen, J.S. et al. CRISPR-Cas12a target binding unleashes indiscriminate
627 single-stranded DNase activity. *Science* **360**, 436-439 (2018).
- 628 16. Gootenberg, J.S. et al. Multiplexed and portable nucleic acid detection
629 platform with Cas13, Cas12a, and Csm6. *Science* **360**, 439-444 (2018).
- 630 17. Li, S.Y. et al. CRISPR-Cas12a-assisted nucleic acid detection. *Cell discovery*
631 **4**, 20 (2018).
- 632 18. Myhrvold, C. et al. Field-deployable viral diagnostics using CRISPR-Cas13.
633 *Science* **360**, 444-448 (2018).
- 634 19. Broughton, J.P. et al. CRISPR–Cas12-based detection of SARS-CoV-2.
635 *Nature biotechnology* (2020).
- 636 20. Ackerman, C.M. et al. Massively multiplexed nucleic acid detection using
637 Cas13. *Nature* (2020).
- 638 21. Hou, T. et al. Development and evaluation of a rapid CRISPR-based
639 diagnostic for COVID-19. *PLOS Pathogens* **16**, e1008705 (2020).
- 640 22. Ding, X. et al. Ultrasensitive and visual detection of SARS-CoV-2 using all-in-
641 one dual CRISPR-Cas12a assay. *Nature communications* **11**, 4711 (2020).
- 642 23. Low, H., Chan, S.-J., Soo, G.-H., Ling, B. & Tan, E.-L. Clarity™ digital PCR
643 system: a novel platform for absolute quantification of nucleic acids. *Analytical*
644 *and Bioanalytical Chemistry* **409**, 1869-1875 (2017).
- 645 24. Li, S.Y. et al. CRISPR-Cas12a has both cis- and trans-cleavage activities on
646 single-stranded DNA. *Cell research* **28**, 491-493 (2018).
- 647 25. Li, J., Macdonald, J. & von Stetten, F. Review: a comprehensive summary of
648 a decade development of the recombinase polymerase amplification. *The*
649 *Analyst* **144**, 31-67 (2018).
- 650 26. Chen, J., Kadlubar, F.F. & Chen, J.Z. DNA supercoiling suppresses real-time
651 PCR: a new approach to the quantification of mitochondrial DNA damage and
652 repair. *Nucleic acids research* **35**, 1377-1388 (2007).
- 653 27. Hou, Y., Zhang, H., Miranda, L. & Lin, S. Serious Overestimation in
654 Quantitative PCR by Circular (Supercoiled) Plasmid Standard: Microalgal
655 pcna as the Model Gene. *PLoS one* **5**, e9545 (2010).
- 656 28. Beinhauerova, M., Babak, V., Bertasi, B., Boniotti, M.B. & Kralik, P. Utilization
657 of Digital PCR in Quantity Verification of Plasmid Standards Used in
658 Quantitative PCR. *Frontiers in Molecular Biosciences* **7** (2020).
- 659 29. Dong, L., Meng, Y., Wang, J. & Liu, Y. Evaluation of droplet digital PCR for
660 characterizing plasmid reference material used for quantifying ammonia
661 oxidizers and denitrifiers. *Anal Bioanal Chem* **406**, 1701-1712 (2014).
- 662 30. Dong, L. et al. Comparison of four digital PCR platforms for accurate
663 quantification of DNA copy number of a certified plasmid DNA reference
664 material. *Scientific reports* **5**, 13174 (2015).

- 665 31. Elbe, S. & Buckland-Merrett, G. Data, disease and diplomacy: GISAID's
666 innovative contribution to global health. *Global Challenges* **1**, 33-46 (2017).
- 667 32. Shu, Y. & McCauley, J. GISAID: Global initiative on sharing all influenza data
668 – from vision to reality. *Eurosurveillance* **22**, 30494 (2017).
- 669 33. Clancy, E. et al. Development of a rapid recombinase polymerase
670 amplification assay for the detection of *Streptococcus pneumoniae* in whole
671 blood. *BMC infectious diseases* **15**, 481 (2015).
- 672 34. Rohrman, B. & Richards-Kortum, R. Inhibition of recombinase polymerase
673 amplification by background DNA: a lateral flow-based method for enriching
674 target DNA. *Analytical chemistry* **87**, 1963-1967 (2015).
- 675 35. Pujadas, E. et al. SARS-CoV-2 viral load predicts COVID-19 mortality. *The*
676 *Lancet. Respiratory medicine* (2020).
- 677 36. Zheng, S. et al. Viral load dynamics and disease severity in patients infected
678 with SARS-CoV-2 in Zhejiang province, China, January-March 2020:
679 retrospective cohort study. *BMJ* **369**, m1443-m1443 (2020).
- 680 37. Zou, L. et al. SARS-CoV-2 Viral Load in Upper Respiratory Specimens of
681 Infected Patients. *New England Journal of Medicine* **382**, 1177-1179 (2020).
- 682 38. Wölfel, R. et al. Virological assessment of hospitalized patients with COVID-
683 2019. *Nature* **581**, 465-469 (2020).
- 684 39. Hu, F. et al. Smartphone-Based Droplet Digital LAMP Device with Rapid
685 Nucleic Acid Isolation for Highly Sensitive Point-of-Care Detection. *Analytical*
686 *chemistry* **92**, 2258-2265 (2020).
- 687 40. Lin, X., Huang, X., Urmann, K., Xie, X. & Hoffmann, M.R. Digital Loop-
688 Mediated Isothermal Amplification on a Commercial Membrane. *ACS sensors*
689 **4**, 242-249 (2019).
- 690 41. Ma, Y.D. et al. Digital quantification of DNA via isothermal amplification on a
691 self-driven microfluidic chip featuring hydrophilic film-coated
692 polydimethylsiloxane. *Biosensors & bioelectronics* **99**, 547-554 (2018).
- 693 42. Zhao, Y., Chen, F., Li, Q., Wang, L. & Fan, C. Isothermal Amplification of
694 Nucleic Acids. *Chemical reviews* **115**, 12491-12545 (2015).
- 695 43. Daher, R.K., Stewart, G., Boissinot, M., Boudreau, D.K. & Bergeron, M.G.
696 Influence of sequence mismatches on the specificity of recombinase
697 polymerase amplification technology. *Mol Cell Probes* **29**, 116-121 (2015).
- 698 44. Hardinge, P. & Murray, J.A.H. Reduced False Positives and Improved
699 Reporting of Loop-Mediated Isothermal Amplification using Quenched
700 Fluorescent Primers. *Scientific reports* **9**, 7400 (2019).
- 701 45. Kellner, M.J., Koob, J.G., Gootenberg, J.S., Abudayyeh, O.O. & Zhang, F.
702 SHERLOCK: nucleic acid detection with CRISPR nucleases. *Nature protocols*
703 **14**, 2986-3012 (2019).
- 704 46. Lucia, C., Federico, P.-B. & Alejandra, G.C. An ultrasensitive, rapid, and
705 portable coronavirus SARS-CoV-2 sequence detection method based on
706 CRISPR-Cas12. *bioRxiv*, 2020.2002.2029.971127 (2020).
- 707 47. Armbruster, D.A. & Pry, T. Limit of blank, limit of detection and limit of
708 quantitation. *The Clinical biochemist. Reviews* **29 Suppl 1**, S49-52 (2008).



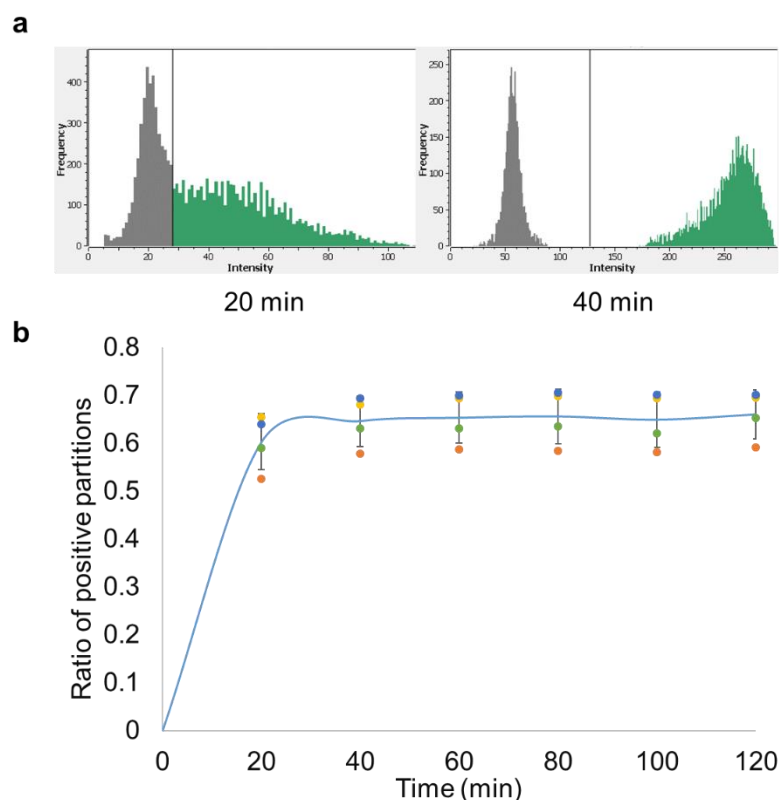
709

710 **Figure 1. Schematic illustration of RADICA. a**, The workflow of RADICA
711 sample partitioning on a chip for absolute quantification of nucleic acid
712 targets. Generally, after the DNA/RNA extraction step, different kind of clinical
713 samples can be used for detection and quantification of various targets. The
714 sample mixture containing DNA/cDNA, RPA reagents, and Cas12a-crRNA-
715 FQ probes is distributed randomly into thousands of partitions. In each
716 partition, the DNA is amplified by RPA and detected by Cas12a-crRNA,
717 resulting in a fluorescent signal in the partition. Based on the proportion of
718 positive partitions and on Poisson distribution, the absolute copy number of
719 the nucleic acid target is quantified. **b**, Illustration of RPA-Cas12a reaction in
720 each positive partition. In each partition containing the target nucleic acid, the
721 primers bind to the target nucleic acid and initiate amplification with the aid of
722 recombinase and DNA polymerase. Because of the strand displacement of
723 DNA polymerase, the exposed crRNA-targeted ssDNA sites are bound by
724 Cas12a-crRNA complexes. Cas12a is then activated and cleaves the nearby
725 FQ reporters to produce a fluorescence readout.



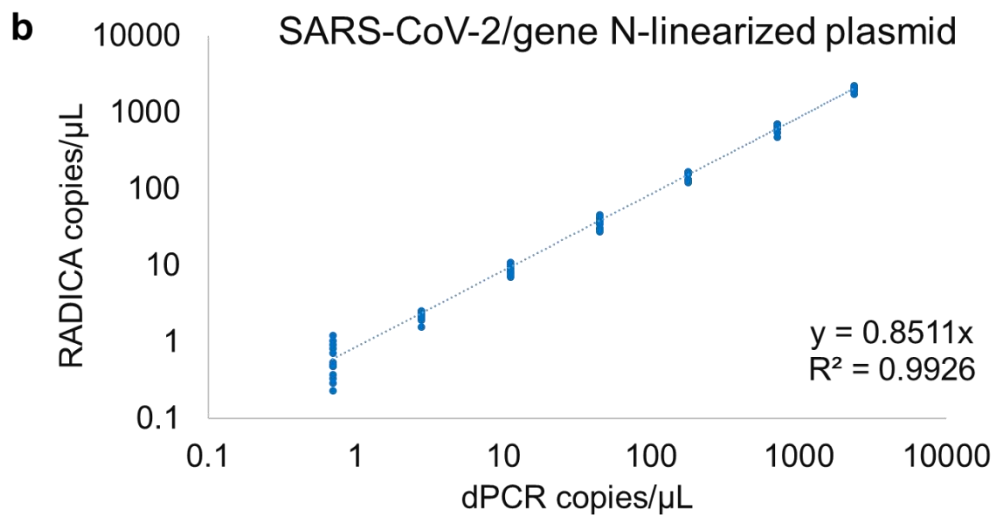
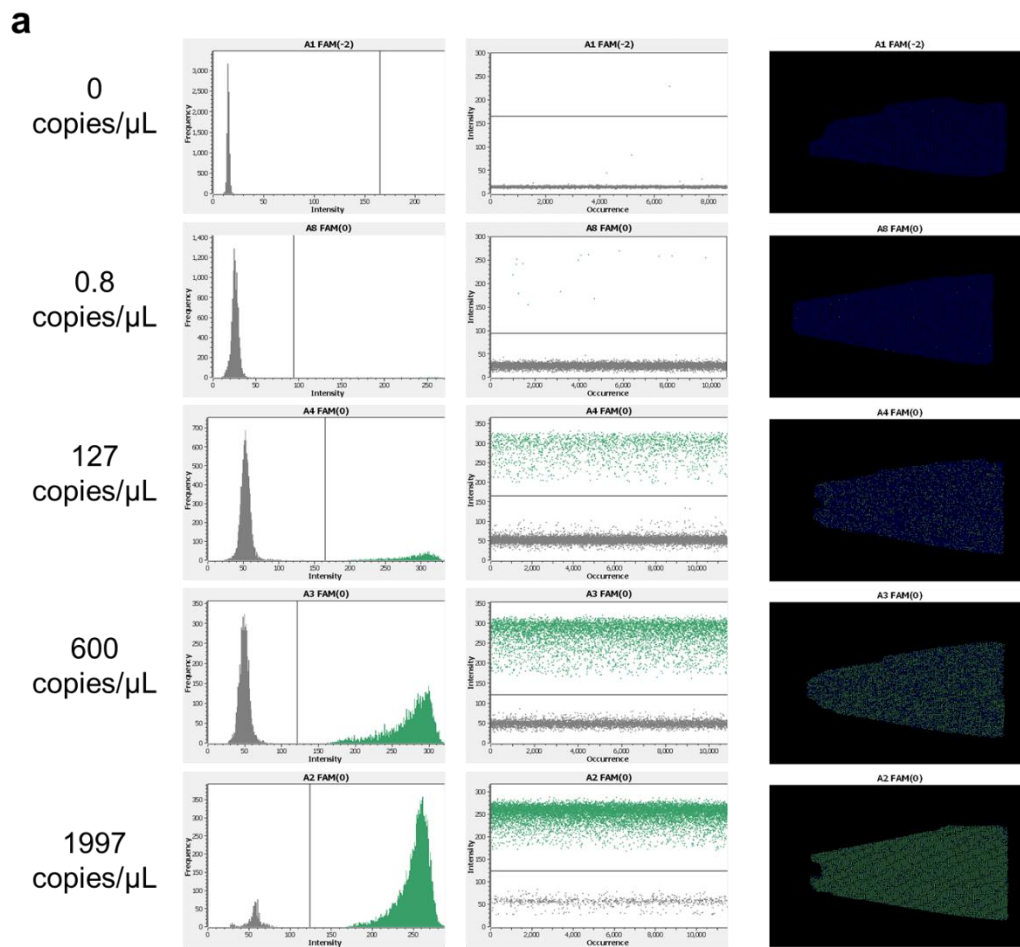
726

727 **Figure 2. Optimization of FQ probe concentration in RADICA. a, b,**
728 Cas12a reaction in bulk reactions with different FQ probe concentrations in
729 the presence or absence of a constant concentration (0.1 nM) of target DNA.
730 **a,** Time course reaction of Cas12a with FQ probes at concentrations ranging
731 from 50 nM to 10,000 nM. X-axis indicates the reaction time; y-axis indicates
732 the background-subtracted fluorescence signal. **b,** Fluorescence signal of
733 DNA and non-template control obtained with FQ probes at concentrations
734 ranging from 50 nM to 10,000 nM. **c, d,** RADICA reaction with the same
735 concentrations of target DNA but different probe concentrations. **c,**
736 Fluorescence intensity of the negative partitions (background noise) and
737 positive partitions (positive signals) on the chip obtained with FQ probes at
738 concentrations of 500 or 1000 nM. **d,** Histogram showing ratios of positive
739 partitions on the chip with FQ probes, at concentrations of 500 or 1000 nM, in
740 the presence of target DNA (4 replicates for each FQ probe concentration).



741

742 **Figure 3. Time course reaction of RADICA. a,** Fluorescence intensity of the
743 partitions on the chip at two time points. The x-axis represents fluorescence
744 intensity while the y-axis represents the frequency of the partitions. The left
745 peak (low fluorescence level; dark grey) on the fluorescence intensity
746 histogram represents the negative partitions while the right peak (high
747 fluorescence level; green) indicates the positive partitions. As the CRISPR
748 reaction proceeds, the fluorescence levels of the positive partitions increase
749 and the right peak shifts further to the right. **b,** The proportion of positive
750 partitions at different time points of RADICA. Each DNA replicate is
751 represented by a data point with a unique color. Starting at about 60 minutes,
752 the fluorescence signal plateaus and the ratio of positive partitions reaches a
753 stable level.



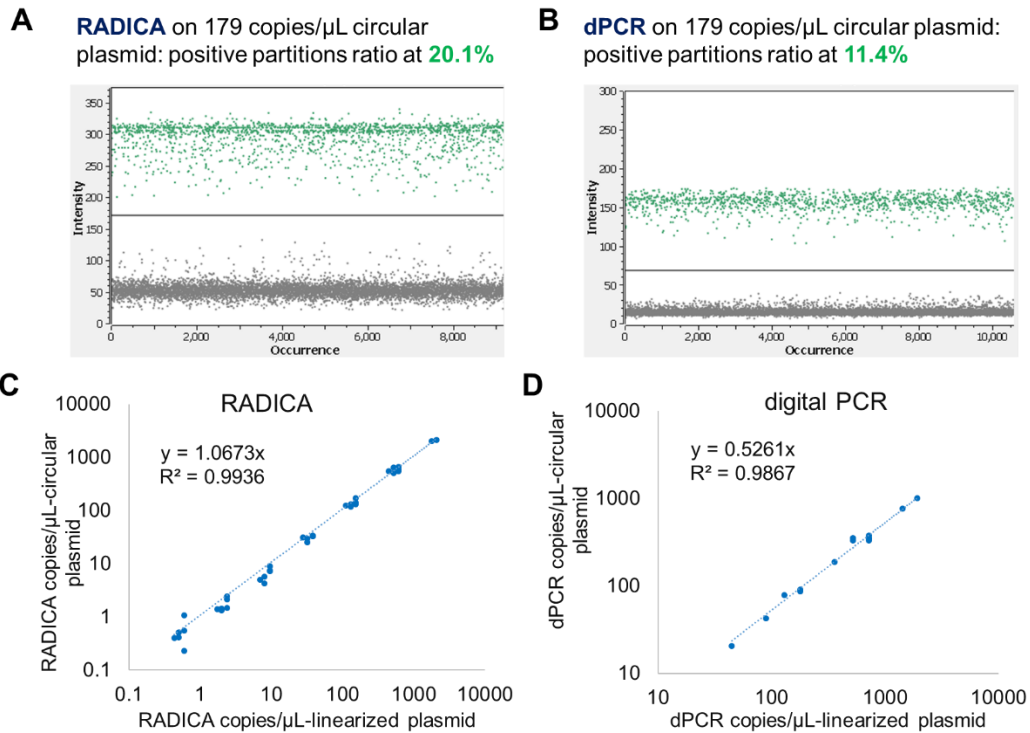
754

755 **Figure 4. RADICA-based detection of different concentrations of SARS-**

756 **CoV-2 N gene DNA. a, Fluorescence intensity histogram, scatter plot, and**

757 **position plot of the partitions on the chip for serial dilutions of DNA. Four**

758 dilutions of linearized plasmid DNA encoding the SARS-CoV-2 N gene (0.8,
759 127, 600, 1997 copies/ μ L) and one non-template control (without plasmid
760 DNA) were used as input DNA. The x-axis represents fluorescence intensity
761 while the y-axis represents the frequency of the partitions. The left peak (low
762 fluorescence level; dark grey) on the fluorescence intensity histogram
763 represents the negative partitions while the right peak (high fluorescence
764 level; green) indicates the positive partitions. In the scatter plot and position
765 plot, each dot represents one partition on the chip. Green dots represent
766 positive partitions with a high fluorescence level while grey or blue dots
767 correspond to negative partitions with a low fluorescence level. **b**, Comparison
768 of the absolute quantification result of RADICA and digital PCR. Each point
769 represents one sample. The original linearized plasmid DNA concentration
770 was measured by using Clarity™ digital PCR and diluted to different
771 concentrations (x-axis). The diluted DNA was then measured by using the
772 RADICA. The calculated RADICA DNA concentrations are plotted on the y-
773 axis.



774

775 **Figure 5. The effect of plasmid conformation on the accuracy of RADICA**
776 **and digital PCR (dPCR). a, b,** The positive and negative partitions of
777 RADICA (a) and dPCR (b) on detection of 179 copies/ μ L circular plasmid. c,
778 d, Comparison of the absolute quantification result for linearized plasmid and
779 circular plasmid of RADICA (c) and dPCR (d).

